Data-driven Time-varying Inertia Estimation of Inverter-based Resources

Bendong Tan, *Student Member, IEEE*, Junbo Zhao, *Senior Member, IEEE*

***Abstract*—This letter proposes a data-driven inertia estimator for inverter-based resources (IBRs) with grid-forming control. It is able to track both constant and time-varying inertia. By utilizing the Thevenin equivalent, the virtual frequency inside IBRs is first estimated with only its terminal voltage and current phasor measurements. The virtual frequency and the measurements are then used together to derive the state-space swing equation model. Then, an enhanced adaptive Unscented Kalman filter (EAUKF) is developed to estimate IBR inertia. Numerical results on the modified IEEE 39-bus power system demonstrate that the proposed inertia estimator remarkably outperforms the existing state-of-art methods both in tracking speed and accuracy.**

***Index Terms*—Inertia estimation, virtual synchronous generator, grid-forming inverters, adaptive Kalman filter.**

I. Introduction

With more and more synchronous generators replaced by inverter-based resources (IBRs), such as wind and solar generations, the inertia of the power system is reduced [1]. Inertia plays a critical role in countering frequency deviations from the nominal value. Accurate knowledge of system real-time inertia is essential for maintaining frequency stability.

To accurately and quickly estimate the inertia inside synchronous generators or regional systems, some methods are proposed using measurements from the phasor measurement units (PMUs) [2]–[4]. To mitigate the frequency instability induced by IBRs, some inverters are equipped with inertia emulation control, i.e., virtual synchronous generator (VSG) control, which may introduce time-varying inertia. [5] develops a dynamic estimator to track the time-varying inertia from VSG, but it suffers from numerical oscillations. [6] utilizes ambient measurements to estimate non-synchronous generator inertia constant, however, it assumes the knowledge of generator rotor speed and angle, difficult to obtain in practice. In addition, it cannot track the time-varying inertia of IBRs due to control parameter changes.

To address the above issues, this paper proposes a data-driven time-varying inertia estimator for IBRs. It only requires the terminal PMU measurements of IBRs and can track both constant and time-varying inertia. Specifically, a Thevenin equivalent of the grid-forming control-based inverter is developed to estimate the virtual frequency. The latter is further utilized to construct and drive the proper state-space model for time-varying inertia tracking. This is achieved by the proposed enhanced adaptive unscented Kalman filter (EAUKF). Numerical results show that the proposed approach can converge quickly and achieve high estimation accuracy.

This work was supported by the U.S. Department of Energy Advanced Grid Modeling (AGM) Program.

B. Tan and J. Zhao are with the Department of Electrical and Computer Engineering, University of Connecticut, Storrs, CT 06269 USA (e-mail: bendong.tan@uconn.edu, junbo@uconn.edu).

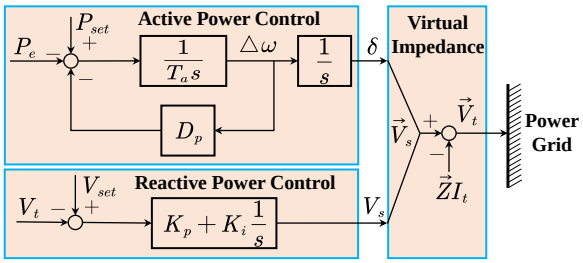

Fig. 1. Control diagram of the VSG-based IBR.

II. Problem Formulation

When an inverter is equipped with virtual synchronous generator (VSG) control, it can provide inertia for frequency support. As shown in Fig. 1, VSG control is mainly composed of three parts: active power control, reactive power control and virtual impedance. P_e and P_{set} are respectively the measured active power and its set point; $\vec{V}_t = V_t\angle\theta$ and V_{set} are respectively the measured terminal voltage and its set point; $\vec{V}_s = V_s\angle\delta$ is the internal voltage of VSG; $\vec{Z} = Z\angle\phi = r_s + jx_s$ is the virtual impedance; $\vec{I}_t$ is the terminal current; ω and δ are respectively the internal virtual frequency and angle; T_a and D_p are the virtual inertia and damping factor respectively, where the virtual inertia plays a similar role as inertia constant in synchronous generators.

The core part of VSG is active power control, which can provide frequency support. Mathematically, it can be formulated as:

$$\begin{cases} \frac{d\delta}{dt} = \Delta\omega = \omega - \omega_s \\ \frac{d\omega}{dt} = \frac{1}{T_a}\left(P_{set} - P_e - D_p \triangle \omega\right) \end{cases} \tag{1}$$

where ω_s is the reference frequency. In (1), we are interested in estimating T_a, which allows us to calculate inertia directly, however, it is a nonlinear and time-varying estimation model under (1) since D_p is also unknown. By linearizing (1), [6] estimates inertia constant but it cannot track time-varying inertia. This letter proposes an online time-varying inertia estimator for VSG control-based inverter.

III. Proposed Time-varying Inertia Estimator

A. Virtual Frequency Estimation

According to (1), T_a and D_p can be easily obtained if the virtual frequency ω is known. Therefore, the first step is to

estimate ω. From Fig. 1, it can be seen that $\vec{V}_s = V_s\angle\delta$ can be derived via Thevenin equivalent:

$$V_s\angle\delta = \vec{V}_t + \vec{Z}\vec{I}_t \tag{2}$$

where ω is the derivatives of δ:

$$\omega = \frac{d\delta}{dt} \tag{3}$$

$\vec{Z}$ can be estimated with recursive total least square in an online manner using our previous approach [7]. In this process, only terminal voltage and current measurements are required. Note that with the reactive power control, V_s will not change violently after a disturbance. Consequently, the estimated $\vec{Z}$ is in turn plugged into (2) to calculate $\vec{V}_s = V_s\angle\delta$ and thereby ω, which will be used as one of the measurements in EAUKF.

B. Time-varying Inertia Estimation based on EAUKF

For synchronous generator inertia constant estimation, damping factor and resistance are negligible [8]. However, in VSG control, the damping factor plays an important role in mitigating the frequency oscillations, while the resistance can also help limit the inverter current. Thus, in this letter, the damping factor and resistance are both estimated when tracking time-varying inertia.

Besides (1), the nonlinear measurement function of active power P_e and reactive power Q_e of VSG can be employed to enhance the estimation tracking:

$$\begin{cases} P_e = \frac{V_s V_t}{Z}\cos(\theta-\delta+\phi) - \frac{V_t^2}{Z}\cos(\phi) \\ Q_e = \frac{V_s V_t}{Z}\sin(\theta-\delta+\phi) - \frac{V_t^2}{Z}\sin(\phi) \end{cases} \tag{4}$$

By taking V_s, T_a and D_p as additional state variables, (1) and (4) can be discretized and cast into Kalman filter framework, where the state space function at time step k can be formulated as:

$$\begin{cases} \omega_k - \omega_{k-1} = \frac{\Delta t}{T_{a,k-1}}\left[P_{set} - \tilde{P}_{e,k-1} - D_{k-1}\triangle\omega_{k-1}\right] + \epsilon_{k1} \\ \delta_k - \delta_{k-1} = (\omega_{k-1}-\omega_s)\Delta t + \epsilon_{k2} \\ V_{s,k} = V_{s,k-1} + \epsilon_{k3} \\ T_{a,k} = T_{a,k-1} + \epsilon_{k4} \\ D_{p,k} = D_{p,k-1} + \epsilon_{k5} \end{cases} \tag{5}$$

$$\tilde{P}_{e,k} = \frac{V_{s,k}V_{t,k}}{Z_k}\cos(\theta_k-\delta_k+\phi_k) - \frac{V_{t,k}^2}{Z_k}\cos(\phi_k) \tag{6}$$

while the measurement function is written as:

$$\begin{cases} z_{k1} = \frac{d\delta}{dt} = \omega_k + \upsilon_{k1} \\ z_{k2} = \frac{V_{s,k}V_{t,k}}{Z_k}\cos(\theta_k-\delta_k+\phi_k) - \frac{V_{t,k}^2}{Z_k}\cos(\phi_k) + \upsilon_{k2} \\ z_{k3} = \frac{V_{s,k}V_{t,k}}{Z_k}\sin(\theta_k-\delta_k+\phi_k) - \frac{V_{t,k}^2}{Z_k}\sin(\phi_k) + \upsilon_{k3} \end{cases} \tag{7}$$

where Δt is the time step; z_{k1}, z_{k2} and z_{k3} are respectively the measurement functions of ω_k, $P_{e,k}$ and $Q_{e,k}$; $\boldsymbol{\epsilon_k} = [\epsilon_{k1}\ \epsilon_{k2}\ \epsilon_{k3}\ \epsilon_{k4}\ \epsilon_{k5}]^\mathsf{T}$ and $\boldsymbol{\upsilon_k} = [\upsilon_{k1}\ \upsilon_{k2}\ \upsilon_{k3}]^\mathsf{T}$ are process noise and measurement noise respectively, which are assumed to be zero-mean white Gaussian noise with covariance matrices $\boldsymbol{Q}_k = \mathrm{E}[\boldsymbol{\epsilon}_k\boldsymbol{\epsilon}_k^\mathsf{T}]$ and $\boldsymbol{R}_k = \mathrm{E}[\boldsymbol{\upsilon}_k\boldsymbol{\upsilon}_k^\mathsf{T}]$.

(5) and (7) can be simplified with the discretized state space function $\boldsymbol{f}(\cdot)$ and the discretized measurement function $\boldsymbol{h}(\cdot)$.

$$\begin{cases} \boldsymbol{x}_k = \boldsymbol{f}(\boldsymbol{x}_{k-1}, \boldsymbol{u}_k) + \boldsymbol{\epsilon}_k \\ \boldsymbol{z}_k = \boldsymbol{h}(\boldsymbol{x}_k, \boldsymbol{u}_k) + \boldsymbol{\upsilon}_k \end{cases} \tag{8}$$

where $\boldsymbol{x} \in \mathbb{R}^{n\times 1}$ is the n-dimension state variable vector and $\boldsymbol{z} \in \mathbb{R}^{m\times 1}$ is the m-dimension measurement variable vector. Specifically, for $\boldsymbol{x}$ and $\boldsymbol{z}$ at time step k, they can be respectively written as $\boldsymbol{x}_k = [\omega_k\ \delta_k\ V_{s,k}\ T_{a,k}\ D_{p,k}]^\mathsf{T}$ and $\boldsymbol{z}_k = [z_{k1}\ z_{k2}\ z_{k3}]^\mathsf{T}$; $\boldsymbol{u_k} = [V_{t,k}\ \theta_k]^\mathsf{T}$ is the input variable vector.

To achieve online inertia estimation, the EAUKF is proposed. EAUKF at time step k consists of three steps: prediction step, updating step and noise covariance matrices adaptation step, which are summarized below

1) Prediction step: With the state vector $\widehat{\boldsymbol{x}}_{k-1}$ and its covariance matrix $\boldsymbol{\Sigma}_{k-1}^{xx}$ at time step $k-1$, $2n$ weighted sigma points $\boldsymbol{\chi}_{k-1}$with weight $w_j = 1/(2n)$ can be generated and propagated via the nonlinear system to obtain the predicted state $\widehat{\boldsymbol{x}}_{k|k-1}$ and its corresponding covariance matrix $\boldsymbol{\Sigma}_{k|k-1}^{xx}$:

$$\begin{cases} \boldsymbol{\chi}_{k-1}^j = \widehat{\boldsymbol{x}}_{k-1} \pm \left(\sqrt{n\boldsymbol{\Sigma}_{k-1}^{xx}}\right)_j, j = 1, 2, \cdots, 2n \\ \boldsymbol{\chi}_{k|k-1}^j = \boldsymbol{f}(\boldsymbol{\chi}_{k-1}^j) \\ \widehat{\boldsymbol{x}}_{k|k-1} = \sum_{j=1}^{2n} w_j \boldsymbol{\chi}_{k|k-1}^j; \boldsymbol{e}_{k|k-1}^{xx,j} = \widehat{\boldsymbol{\chi}}_{k|k-1}^j - \widehat{\boldsymbol{x}}_{k|k-1} \\ \boldsymbol{\Sigma}_{k|k-1}^{xx} = \sum_{j=1}^{2n} w_j \left(\boldsymbol{e}_{k|k-1}^{xx,j}\right)\left(\boldsymbol{e}_{k|k-1}^{xx,j}\right)^\mathsf{T} + \boldsymbol{Q}_k \\ \widehat{\boldsymbol{\chi}}_{k|k-1}^j = \widehat{\boldsymbol{x}}_{k|k-1} \pm \left(\sqrt{n\boldsymbol{\Sigma}_{k|k-1}^{xx}}\right)_j, j = 1, 2, \cdots, 2n \\ \widehat{\boldsymbol{z}}_{k|k-1} = \sum_{j=1}^{2n} w_j \boldsymbol{h}(\widehat{\boldsymbol{\chi}}_{k|k-1}^j); \boldsymbol{e}_{k|k-1}^{zz,j} = \boldsymbol{h}(\widehat{\boldsymbol{\chi}}_{k|k-1}^j) - \widehat{\boldsymbol{z}}_{k|k-1} \end{cases} \tag{9}$$

where $\widehat{\boldsymbol{z}}_{k|k-1}$ is the predicted measurements vector.

2) Updating step: this step is to update state vectors $\widehat{\boldsymbol{x}}_k$ and its covariance matrix $\boldsymbol{\Sigma}_k^{xx}$ at time step k.

$$\begin{cases} \boldsymbol{\Sigma}_{k|k-1}^{zz} = \sum_{j=1}^{2n} w_j \left(\boldsymbol{e}_{k|k-1}^{zz,j}\right)\left(\boldsymbol{e}_{k|k-1}^{zz,j}\right)^\mathsf{T} + \boldsymbol{R}_k \\ \boldsymbol{\Sigma}_{k|k-1}^{xz} = \sum_{j=1}^{2n} w_j \left(\widehat{\boldsymbol{\chi}}_{k|k-1}^j - \widehat{\boldsymbol{x}}_{k|k-1}\right)\left(\boldsymbol{h}(\widehat{\boldsymbol{\chi}}_{k|k-1}^j) - \widehat{\boldsymbol{z}}_{k|k-1}\right)^\mathsf{T} \\ \mathbf{K}_k = \boldsymbol{\Sigma}_{k|k-1}^{xz}(\boldsymbol{\Sigma}_{k|k-1}^{zz})^{-1} \\ \widehat{\boldsymbol{x}}_k = \widehat{\boldsymbol{x}}_{k|k-1} + \mathbf{K}_k(\boldsymbol{z}_k - \widehat{\boldsymbol{z}}_{k|k-1}) \\ \boldsymbol{\Sigma}_k^{xx} = \boldsymbol{\Sigma}_{k|k-1}^{xx} + \mathbf{K}_k\boldsymbol{\Sigma}_{k|k-1}^{zz}\mathbf{K}_k^\mathsf{T} \end{cases} \tag{10}$$

3) Noise covariance matrices adaptation step: since process noise $\boldsymbol{Q}_k$ and measurement noise $\boldsymbol{R}_k$ are time-varying, their corresponding covariance matrices should be adaptively updated. This paper adopts the following approach:

$$\begin{cases} \boldsymbol{C}_k = \frac{\sum_{i=k-L+1}^{k}(\boldsymbol{z}_i - \boldsymbol{h}(\widehat{\boldsymbol{x}}_i))(\boldsymbol{z}_i - \boldsymbol{h}(\widehat{\boldsymbol{x}}_i))^\mathsf{T}}{L} \\ \alpha = (1-\beta)/(1-\beta^k); \boldsymbol{d}_k = \boldsymbol{z}_k - \widehat{\boldsymbol{z}}_{k|k-1} \\ \boldsymbol{Q}_{k+1} = (1-\alpha)\boldsymbol{Q}_k + \alpha\mathbf{K}_k\boldsymbol{C}_k\mathbf{K}_k^\mathsf{T} \\ \boldsymbol{R}_{k+1} = \gamma\boldsymbol{R}_k + (1-\gamma)\boldsymbol{d}_k\boldsymbol{d}_k^\mathsf{T} \end{cases} \tag{11}$$

where $\boldsymbol{C}_k$ and $\boldsymbol{d}_k$ are measurement estimation error covariance and residual, respectively; L is the length of measurements used to update noise covariance matrices; both $\beta \in [0.95\ 1]$ and $\gamma \in [0.9\ 1]$ are constant.

For virtual inertia tracking of the grid-following inverter, its

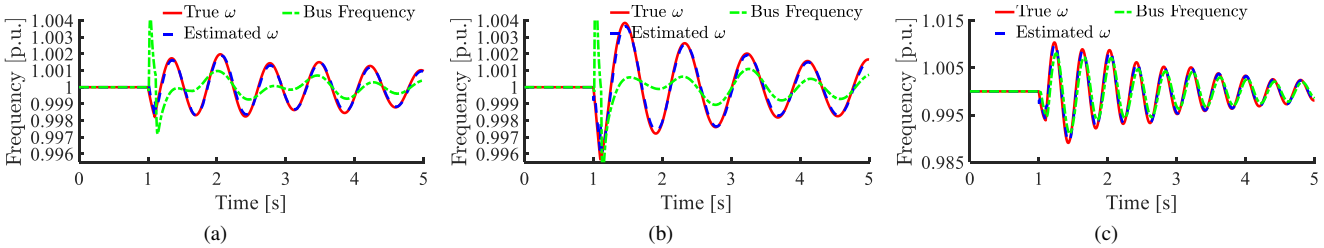

Fig. 2. Virtual frequency estimation of VSG under various scenarios. (a) Scenario 1; (b) Scenario 2; (c) Scenario 3.

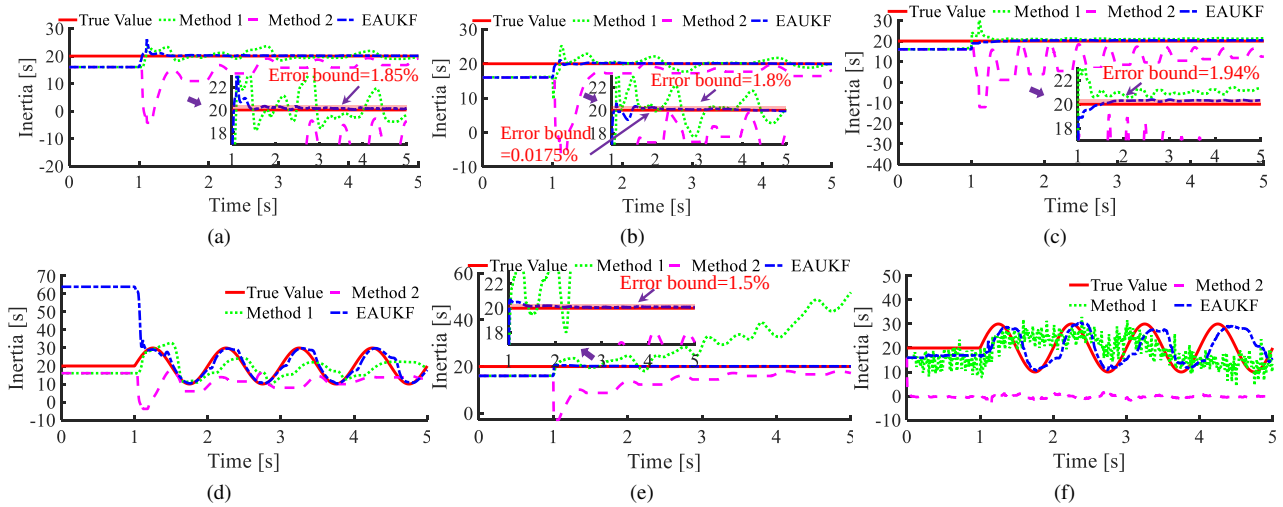

Fig. 3. Inertia estimation results under various scenarios. (a) Scenario 1; (b) Scenario 2; (c) Scenario 3; (d) Scenario 4; (e) Scenario 5; (f) Scenario 6.

active power control can be formulated as [1]:

$$\begin{cases} \frac{d\theta}{dt} = \Delta f = f - f_s \\ \frac{df}{dt} = \frac{1}{K_d}\left(P_{set} - P_e - K_e \Delta f\right) \end{cases} \tag{12}$$

where f and f_s are respectively the bus terminal frequency and its nominal value, while K_d and K_e are respectively the control coefficients. By replacing (1) with (12) and calculating δ with (2), the same Kalman filter framework can also be applied for the estimation of K_d and K_e.

IV. Numerical Results

The proposed inertia estimator is tested using the modified IEEE 39-bus power system, where Bus 4 is connected with 80MW VSG control-based inverter. For VSG control, D_p is 20, while the control parameters K_p and K_i are respectively set as 0.5 and 0. The following scenarios are investigated to verify the performance of the proposed method:

- **Scenario 1**: Constant inertia $H = \frac{1}{2}T_a = 20$ s, virtual reactance $x_s = 0.106$ pu and and small virtual resistance $r_s = 0.006$ pu;
- **Scenario 2**: Constant inertia $H = \frac{1}{2}T_a = 20$ s, virtual reactance $x_s = 0.106$ pu and large virtual resistance $r_s = 0.1$ pu;
- **Scenario 3**: Constant inertia $H = \frac{1}{2}T_a = 20$ s, virtual reactance $x_s = 0.006$ pu and virtual resistance $r_s = 0.006$ pu;
- **Scenario 4**: Time-varying inertia $H = \frac{1}{2}T_a = 10(\sin[2\pi(t-1)] + 2)$ s, virtual reactance $x_s = 0.106$ pu and virtual resistance $r_s = 0.006$ pu, where the sin function is used to emulate time-varying inertia.

For Scenarios 1 to 4, a three-phase short-circuit fault is applied to Bus 3 at $t = 1$ s and is cleared at $t = 1.1$ s. To evaluate the impacts of different disturbance natures and noises on the proposed inertia estimator, Scenarios 5 and 6 are also tested:

- **Scenario 5**: Constant inertia $H = \frac{1}{2}T_a = 20$ s, virtual reactance $x_s = 0.106$ pu and small virtual resistance $r_s = 0.006$ pu; the load on Bus 4 is tripped at $t = 1$ s;
- **Scenario 6**: Time-varying inertia $H = \frac{1}{2}T_a = 10(\sin[2\pi(t-1)] + 2)$ s, virtual reactance $x_s = 0.106$ pu and virtual resistance $r_s = 0.006$ pu; a three-phase short-circuit fault is applied to Bus 3 at $t = 1$ s and is cleared at $t = 1.1$ s; according to IEEE standard, 1% total vector error is simulated by adding mean-zero Gaussian noise with standard deviation [9], [10]

$$\sigma = \frac{\mathrm{E}[\varpi] \times 1\%}{3 \times 100} \tag{13}$$

where ϖ denotes measurements.

In all scenarios, L is 10, β is 0.99 while γ is 0.95. Besides, the state-of-art methods in [8] (Method 1) and [5] (Method 2) are compared. The initial value of ω, δ, and V_s can be obtained from the power flow solutions-based initialization that is widely used in power system transient simulations. The initial values of T_a and D_p are 80% of their true values for Scenarios 1-3 and 5-6, while 320% of the true values for Scenario 4. These different initialization errors would be used to demonstrate the robustness of the proposed method.

A. Necessity for Virtual Frequency Estimation

It is worth noting that for existing inertia estimation works on the synchronous generator, i.e., [2], the generator terminal bus frequency is usually utilized as the approximation of rotor speed. This approximation may be acceptable when the internal impedance of synchronous generators is small, and this is also true for small-impedance VSG, as shown in Fig. 2(c). However, as VSG requires a large virtual impedance to mitigate inverter current, it will lead to a large estimation bias for VSG, as shown in Figs. 2(a)-(b). Therefore, virtual frequency estimation for VSG is necessary. From Figs. 2(a)-(b), it can be seen that, with a larger resistance, the frequency dynamics will be more violent. However, the virtual frequency inside VSG can be accurately estimated in each scenario by the proposed method.

B. Performance Comparisons under Different Scenarios

Figs. 3(a)-(d) show the inertia estimation results of different methods under various scenarios. It can be observed that in Scenarios 1, 2 and 3, the proposed EAUKF can converge within 0.5 seconds with the maximum error of 1.94% and can track the time-varying inertia timely and accurately with the help of the adaptiveness of $\boldsymbol{Q}_k$ and $\boldsymbol{R}_k$. However, since Method 1 doesn't consider the damping factor, which has non-negligible impacts on frequency, the estimation error is more than 18%. For Method 2, it can be seen that its maximum estimation error is up to 50% and it fails to track time-varying inertia. It is worth pointing out that Method 2 is subject to numerical oscillations especially when the virtual resistance is small. This is because the dynamic estimator in Method 2 also cannot estimate the damping factor well, which has been shown in [5]. On the other hand, by comparing Method 1 with EAUKF, it can be shown that the adaptive adjustment of $\boldsymbol{Q}_k$ and $\boldsymbol{R}_k$ is critical to enhancing its capability of handling both constant and time-varying inertia.

C. Robustness Validation

Comparing the results shown in Fig. 3(d) with those in Fig. 3, it can be found that the proposed method can still achieve accurate and fast inertia tracking even with 220% error of initial values, which indicates the proposed estimator is not sensitive to the initial values; it can also be seen from Fig. 3(e) that the proposed inertia estimator is able to handle different dynamic events of various natures, while Method 1 diverges in Scenario 5, which may be due to the significant impacts of damping factor; Fig. 3(f) demonstrates that the proposed method is only slightly affected by noise thanks to the adaptiveness of $\boldsymbol{Q}_k$ and $\boldsymbol{R}_k$, although there is an estimation time delay. However, with measurement noise, Methods 1 and 2 fail, demonstrating the superiority of the proposed inertia estimator. These illustrate the applicability of the proposed method for the practical power system.

V. Conclusions

This letter proposes a data-driven online time-varying estimator for VSG control-based inverter using IBR terminal voltage and current phasor measurements. Specifically, the virtual frequency inside VSG is estimated via Thevenin equivalent in a real-time manner. By modeling the active power control and deriving the state-space model between unknown states and parameters to the measurements, the EAUKF is proposed to track the time-varying inertia. Numerical results on the IEEE 39-bus power system show that the proposed method is able to track both constant and time-varying inertia accurately and quickly and achieves significantly superior performance compared with existing state-of-art methods. Future works will be extending the developed approach to consider the current limiter impacts of IBRs, improving the performance for tracking time-varying inertia and damping parameters as well as testing its effectiveness using field measurements from practical power systems.

References

[1] B. Tan, *et al.*, "Power system inertia estimation: review of methods and the impacts of converter-interfaced generations,", *International Journal of Electrical Power & Energy Systems*, vol. 134, pp. 107362, 2022.

[2] P. M. Ashton, *et al.*, "Inertia estimation of the GB power system using synchrophasor measurements," *IEEE Trans. Power Syst.*, vol. 30, no. 2, pp. 701-709, March 2015.

[3] D. Yang, *et al.*, "Data-driven estimation of inertia for multiarea interconnected power systems using dynamic mode decomposition," *IEEE Trans. Industrial Informatics*, vol. 17, no. 4, pp. 2686-2695, April 2021.

[4] K. Tuttelberg, *et al.*, "Estimation of power system inertia from ambient wide area measurements," *IEEE Trans. Power Syst.*, vol. 33, no. 6, pp. 7249-7257, Nov. 2018.

[5] M. Liu, *et al.*, "On-line inertia estimation for synchronous and non-synchronous devices," *IEEE Trans. Power Syst.*, vol. 36, no. 3, pp. 2693-2701, May 2021.

[6] J. Guo, *et al.*, "Estimation of inertia for synchronous and non-synchronous generators based on ambient measurements," *IEEE Trans. Power Syst.*, vol. 37, no. 5, pp. 3747-3757, Sept. 2022.

[7] L. Peng, *et al.*, "Real-time LCC-HVDC maximum emergency power capacity estimation based on local PMUs," *IEEE Trans. Power Syst.*, vol. 36, no. 2, pp. 1049-1058, 2021.

[8] B. Tan, *et al.*, "Decentralized data-driven estimation of generator rotor speed and inertia constant based on adaptive unscented Kalman filter,", *International Journal of Electrical Power & Energy Systems*, vol. 137, 2022.

[9] "IEEE standard for synchrophasor measurements for power systems," IEEE Std C37.118.1-2011, pp.1-61, Dec. 2011.

[10] R. Singh, *et al.*, "Choice of estimator for distribution system state estimation". *IET Generation, Transmission & Distribution.*, vol. 3, no. 7, pp. 666, 2009.